Vector Analysis of Optical Dielectric Waveguide Bends Using Finite-Difference Method

Sangin Kim and Anand Gopinath

Abstract— **A full-vectorial analysis of optical dielectric waveguide bends using the finite-difference method has been developed. The formulation was based on the transverse electric field components, E_r and E_z. To set up the boundary conditions at each dielectric interface, the continuity of E_θ, H_θ, and the tangential component of the electric field, and the discontinuity of the normal component of the electric field were satisfied. The finite-difference scheme was modified to satisfy these boundary conditions. The results of the analysis using the current method is compared with previous results. The optimal offset for 90° bends was obtained, and the losses for these optimal bend structures are also presented.**

I. Introduction

THE design of optical dielectric waveguide bends is important in integrated photonic devices. It is desirable to use low-loss bends with small radii of curvature, as substitutes for T-junctions with deep etched mirrors in bifurcators or corner bends with mirrors. The problem with deep etched mirrors is that they are difficult to build: small dislocation or tilt of mirror increases loss, and the mirror cannot be used for buried waveguide structures. The bend does not suffer from these problems, and is the only possible structure for the buried structures. For these reasons, accurate calculation of loss of optical dielectric waveguide bends is very important.

Since Marcatili published the first theoretical paper on bends in optical dielectric guides in 1969 [1], a large number of methods have been developed to analyze waveguide bends. Heiblum and Harris [2] used the conformal transformation method in which the curved waveguide is translated into an equivalent straight waveguide with a transformed index profile. Gu *et al.* [3], [4] analyzed a curved ridge waveguide using the method of lines (MoL). In their work, the waveguide is discretized in axial direction and in each region, the field is expressed with a set of Bessel and Hankel functions. While the methods mentioned above are based on the analytic solutions, one of the numerical methods, the scalar finite-element method (SFEM) has been also applied to curved waveguides as well as straight ones [5]–[7]. Vectorial analysis of waveguide bends has been performed using the method of lines by Pregla *et al.* [10], [11], and vectorial analysis of circularly curved channel waveguides with rectangular cross-section has been done using the source-type integral equation method by Blok *et al.* [12].

Manuscript received May 16, 1996; revised June 7, 1996. This work was supported by an ARPA subcontract through SDL Inc. San Jose, CA.

The authors are with the Department of Electrical Engineering, University of Minnesota, Minneapolis, MN 55455 USA.

Publisher Item Identifier S 0733-8724(96)07050-8.

In this paper, the finite-difference method which has been widely used for the analysis of straight waveguides was applied to the full vector analysis of waveguide bends. To satisfy the boundary conditions at the interfaces where the index profile is discontinuous, the method used by Stern [8] was extended. The loss of waveguide bends was calculated from the imaginary part of the complex angular propagation constant, and from overlap integral between straight waveguide mode and curved waveguide mode to include the loss due to mode mismatch. The minimized loss was also calculated by using offset at the conjunctions between straight waveguide and curved one to reduce the loss due to mode mismatch.

II. Formulation

In the previous analysis of curved waveguides, the scalar formulation or the semivectorial formulation (for instance, Yamamoto *et al.* [7]) was used. In the scalar formulation, only one component of the field was considered in the analysis. In the semivectorial formulation, quasi-TE mode, and quasi-TM mode were calculated, but with additional boundary conditions. However, these formulations cannot be used for the analysis of the hybrid mode, in which all six components of the field exist. In this paper, a full vectorial analysis of the curved waveguides based on a formulation in terms of E_r and E_z components has been carried out. The formulation used the Helmholtz equations for these components, but the E_θ component in E_r equation was eliminated using the divergence condition.

Maxwell equations written in the cylindrical coordinates (r, θ, z) become

$$-j\frac{\nu}{r}E_z - \frac{\partial E_\theta}{\partial z} = -j\omega\mu_0 H_r \tag{1}$$

$$\frac{\partial E_R}{\partial z} - \frac{\partial E_z}{\partial r} = -j\omega\mu_0 H_\theta \tag{2}$$

$$\frac{1}{r}\frac{\partial (rE_\theta)}{\partial r} + j\frac{\nu}{r}E_r = -j\omega\mu_0 H_z \tag{3}$$

$$-j\frac{\nu}{r}H_z - \frac{\partial H_\theta}{\partial z} = j\omega\varepsilon_0 n^2 E_r \tag{4}$$

$$\frac{\partial H_r}{\partial z} - \frac{\partial H_z}{\partial r} = j\omega\varepsilon_0 n^2 E_\theta \tag{5}$$

$$\frac{1}{r}\frac{\partial (rH_\theta)}{\partial r} + j\frac{\nu}{r}H_r = j\omega\varepsilon_0 n^2 E_z \tag{6}$$

$$\frac{1}{r}\frac{\partial (rE_r)}{\partial r} - j\frac{\nu}{r}E_\theta + \frac{\partial E_z}{\partial z} = 0 \tag{7}$$

$$\frac{1}{r}\frac{\partial (rH_r)}{\partial r} - j\frac{\nu}{r}H_\theta + \frac{\partial H_z}{\partial z} = 0 \tag{8}$$

where ν is a complex angular propagation constant and it was assumed that the wave front propagates in θ direction. The last two (7) and (8) came from divergence equations. By simple algebraic manipulation, all other components of electric and magnetic field can be explicitly expressed in terms of E_r and E_z

$$E_\theta = -\frac{j}{\nu}\left[\frac{\partial(rE_r)}{\partial r} + r\frac{\partial E_z}{\partial z}\right] \tag{9}$$

$$H_r = -\frac{1}{\omega\mu_0}\left[\frac{1}{\nu}\frac{\partial^2(rE_r)}{\partial z\,\partial r} + \frac{r}{\nu}\frac{\partial^2 E_z}{\partial z^2} - \frac{\nu}{r}E_z\right] \tag{10}$$

$$H_\theta = \frac{j}{\omega\mu_0}\left(\frac{\partial E_r}{\partial z} - \frac{\partial E_z}{\partial r}\right) \tag{11}$$

$$H_z = \frac{1}{\omega\mu_0 r}\left\{\frac{1}{\nu}\frac{\partial}{\partial r}\left[r\frac{\partial(rE_r)}{\partial r}\right] - \nu E_r + \frac{1}{\nu}\frac{\partial}{\partial r}\left[r^2\frac{\partial E_z}{\partial z}\right]\right\}. \tag{12}$$

By substituting (11), (12) into (4), and (10), (11) into (6), we obtain

$$r^2\frac{\partial^2 E_r}{\partial r^2} + 3r\frac{\partial E_r}{\partial r} + r^2\frac{\partial^2 E_r}{\partial z^2} + (r^2k^2n^2+1)E_r + 2r\frac{\partial E_z}{\partial z} = \nu^2 E_r \tag{13}$$

$$r^2\frac{\partial^2 E_z}{\partial r^2} + r\frac{\partial E_z}{\partial r} + r^2\frac{\partial^2 E_z}{\partial z^2} + r^2k^2n^2E_z = \nu^2 E_z. \tag{14}$$

By substituting $\Psi = rE_r$, $\phi = E_z$ into (13), (14), we obtain

$$r^2\frac{\partial^2\psi}{\partial r^2} + r\frac{\partial\psi}{\partial r} + r^2\frac{\partial^2\psi}{\partial z^2} + r^2k^2n^2\psi + 2r^2\frac{\partial\phi}{\partial z} = \nu^2\psi \tag{15}$$

$$r^2\frac{\partial^2\phi}{\partial r^2} + r\frac{\partial\phi}{\partial r} + r^2\frac{\partial^2\phi}{\partial z^2} + r^2k^2n^2\phi = \nu^2\phi. \tag{16}$$

Above two differential equations may be discretized by the finite-difference method and by writing the discretized equations at each node point of the calculation domain, the following matrix equation is obtained:

$$AX = \nu^2 X \tag{17}$$

where A is a $2N \times 2N$ banded asymmetric matrix (N is a total number of nodes) and X is an eigenvector. The eigenvector represents the values of electric field at each point and looks like the following:

$$X = [\Psi_1, \phi_1, \Psi_2, \phi_2, \cdots, \Psi_N, \phi_N]^T. \tag{18}$$

The node points were numbered in r direction from the lower-left corner of the calculation domain and the discretized differential equations (15) and (16) were written alternatively at each node point to reduce the band width of the matrix A. Equation (17) is a matrix eigenvalue problem, and many methods have been developed to solve this kind of problem. In this paper, the shifted inverse power iteration method [9] was used.

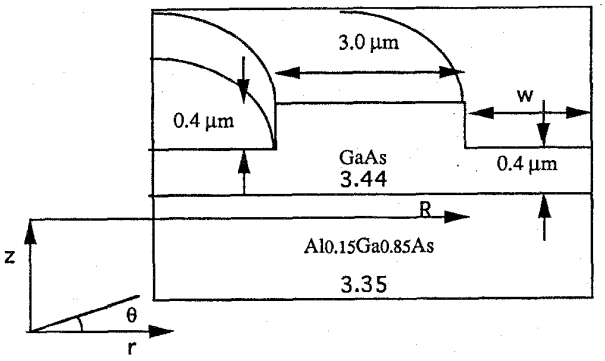

Fig. 1. Configuration of waveguide bend.

III. Boundary Conditions

Fig. 1 shows the configuration of an optical dielectric waveguide bend. The square in Fig. 1 is the outer boundary of the calculation. On the external boundary, the tangential components of the electric field are assumed to satisfy Dirichlet conditions, that is, the tangential component of electric field is zero on the boundary. This condition is equivalent to a perfect conducting boundary. To obtain an accurate result, the boundary was located sufficiently far away from the guiding region.

At the internal interfaces, where index profile is discontinuous, we applied the continuity of E_θ, H_θ, and tangential component of electric field, and also applied the discontinuity of normal component of the electric field. In the Appendix, the finite-difference scheme is modified to satisfy these boundary conditions automatically. However, there is a limit for this method, which is that the internal dielectric interfaces should be parallel to r-axis or z-axis (true for most of the practical waveguide structure).

IV. Numerical Method

The finite-difference mesh was with variable spacing, so that external boundary could be a large distance from the bend. The finite-difference equations including boundary conditions resulted in the matrix equation (17). The results were obtained with a mesh size of 1500 nodes, with 50 points along the r-direction.

To solve the eigenvalue problem, (17), the shifted inverse power iteration method [9] was used. An advantage of this method is that any eigenvalue, not only dominant one, and the corresponding eigenvector may be obtained. To solve the eigenvalue problem, following equations are solved iteratively:

$$(A - pI)V_i = U_i \tag{19}$$

$$U_{i+1} = \frac{V_i}{|V_i|} \tag{20}$$

where p is a scalar constant, I is an identity matrix, and $|V_i|$ represents the norm of the vector V_i. For an arbitrary initial vector, U_0, after enough number of iterations, U_i converges to the required eigenvector and $1/|V_i|$ converges to $|\lambda - p|$ where λ is the corresponding eigenvalue that is closest to p. Equation (19) is a simple linear equation and many subroutines

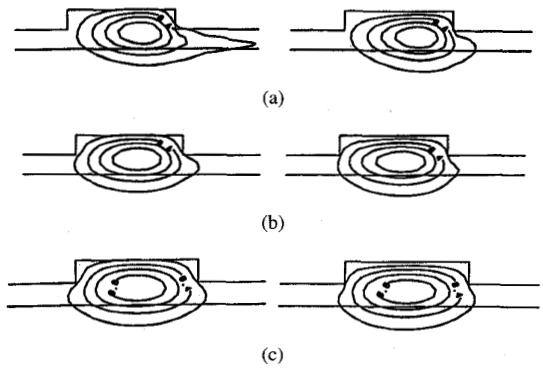

Fig. 2. Contour plots of electric field distributions. (a) Contour plots of E_r (left) and E_z (right) in bend with radius of 200 μm. (b) Contour plots of E_r (left) and E_z (right) in bend with radius of 500 μm. (c) Contour plots of E_r (left) and E_z (right) in straight waveguide.

have been developed to solve this kind of problem. In our calculation, one of the subroutines in IMSL library (in Fortran) was employed.

To test the accuracy of the eigenvalue and the eigenvector, a residual error was calculated, which is defined as $|(A-\lambda I)X|$. In our calculation, the residual error was less then 10^{-8}.

V. Results

The method developed in the above sections was employed to analyze the waveguide bend whose cross section is shown in Fig. 1. A guiding layer, GaAs, is on thick layer, $Al_{0.15}Ga_{0.85}As$. At the wavelength of 1.15 μm, the refractive indexes of GaAs and $Al_{0.15}Ga_{0.85}As$ are 3.44 and 3.35, respectively. Fig. 2(a) shows the contour plots of the r component and the z component of the electric field of the waveguide bend whose radius of curvature is 200 μm, and Fig. 2(b) shows the contour plots of the r component and the z components of the electric field of the waveguide bend whose radius of curvature is 500 μm. The contour plots of quasi-TE and quasi-TM modes of the straight waveguide with the same cross section are shown in Fig. 2(c). We can see that the center of the mode of the waveguide bend shifted to the outer edge of the bend in r direction and the smaller the radius is, the farther the center shifts.

Effective index of waveguide bend can be defined as

$$n_{eff} = \frac{\mathrm{Re}\,(\nu)}{k_0 R} \tag{21}$$

where k_0 is wave number in free space, $2\pi/\lambda$, and R is the radius of curvature of the bend. As shown in Fig. 1, R is defined as the radius of the outer edge of the waveguide bend. Calculated effective index is plotted as a function of radius of curvature in Fig. 3. It is found that as R increases, the effective index of the bend tends to that of the straight waveguide asymptotically.

The loss of 90° bend due to radiation is obtained by

$$L_{rad} = 20\log_{10}\left\{\exp\left[\frac{\pi}{2}\,\mathrm{Im}\,(\nu)\right]\right\}. \tag{22}$$

The radiation loss versus radius of curvature is plotted in Fig. 4. The loss of the same structure was calculated using

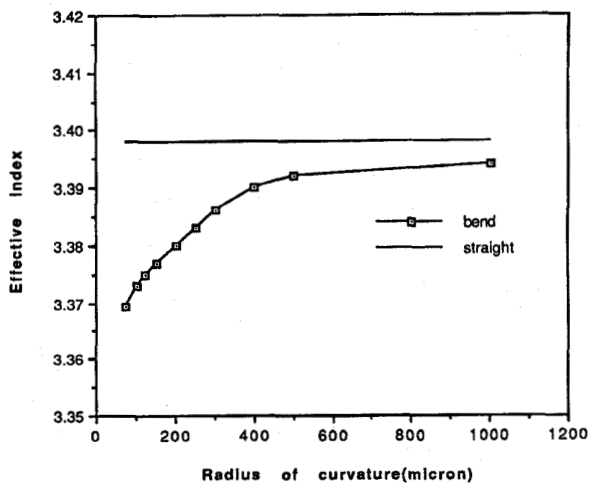

Fig. 3. Plot of effective index of bends versus radius of curvature.

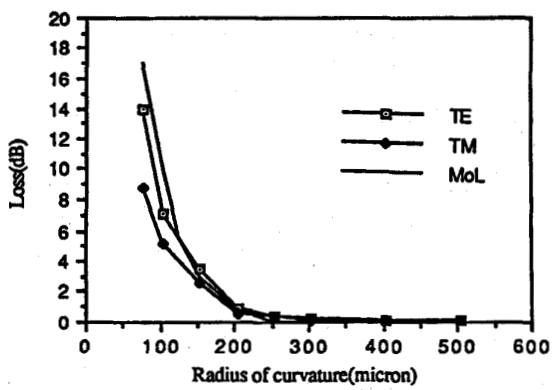

Fig. 4. Plot of radiation loss versus radius of curvature.

MoL by Gu *et al.* [4] and using FEM by Yamamoto *et al.* [7]. The loss calculated by Gu *et al.* [4] is plotted with our result in Fig. 4. Gu's approach is semivectorial and the plotted result in Fig. 4 is for TE polarization. Similar result was also reported by Yamamoto *et al.* [7]. For the large radius of curvature ($R > 200\,\mu$m), our result agrees very well with Gu's. For the radius smaller than 200 μm, our calculated loss shows some difference from Gu's, and we surmise that the difference may be due to the external boundary condition, but we are uncertain about this since changing the distance between the external boundary and the bend edge does not show any difference in radiation losses once the losses are stabilized.

As shown in Fig. 4, the loss for quasi-TE mode is higher than that for quasi-TM mode. This polarization dependence of the loss arises from the tighter confinement of the field in z direction than in r direction for the waveguide structure considered here.

The transition losses of bends due to mode mismatch at various radii of curvature were calculated from the overlap integral. The overlap integrals for two differently polarized inputs, quasi-TE mode and quasi-TM mode, were done separately. Since we assumed both ends of the 90° bend are connected with straight guides, the overlap integral was done twice. The structure considered here is a multimode wave-

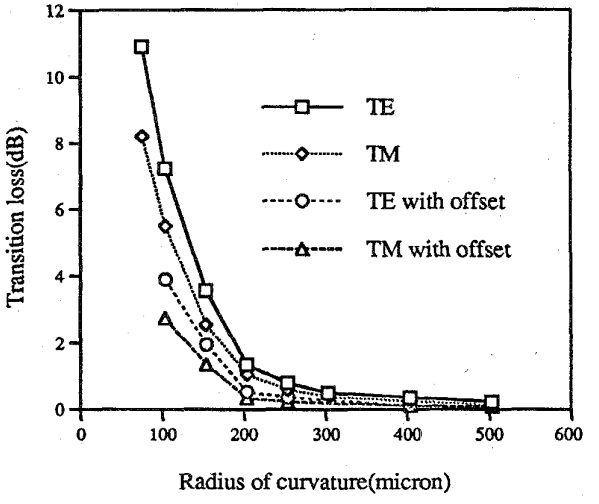

Fig. 5. Plot of transition loss versus radius of curvature.

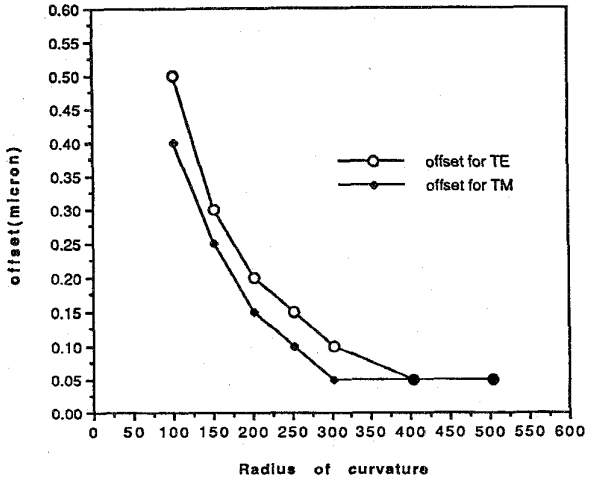

Fig. 6. Plot of the optimal offsets versus radius of curvature.

guide. For the convenience of calculation (for multimode waveguide, we do not know the field distribution at the connection between the straight waveguide and bend), the overlap integral was done using only the fundamental mode of the straight waveguide. The minimized transition loss with optimal offsets at the ends of bend was calculated from the shifted overlap integral. The transition loss and the minimized transition loss with optimal offset were plotted in Fig. 5. To find the optimal offset, we repeated overlap integral with different locations of the straight waveguide. Fig. 6 shows the optimal offsets as a function of the radius of curvature.

In order to investigate the effect of outer boundary location on the calculated loss, similar calculations have been done with different locations of the outer boundary. Fig. 7 shows the plot of calculated losses versus the distance between the outer edge of bend and the vertical external boundary. As seen in Fig. 7, the losses get stable if the outer boundary is located far enough ($>6\,\mu$m). All the losses plotted in Figs. 4 and 5 are calculated by locating the outer boundary at 8 μm away from the outer edge of the bend.

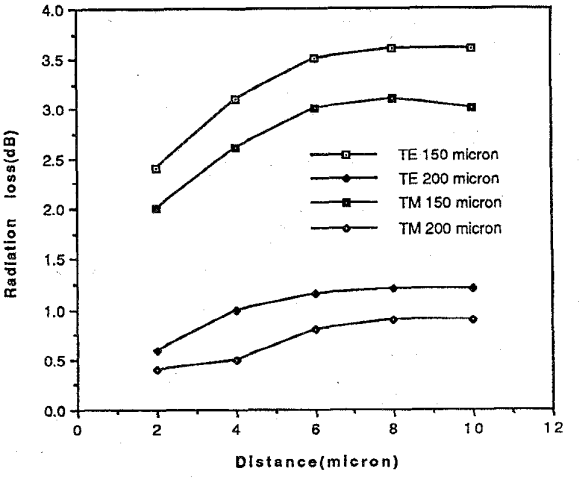

Fig. 7. Plot of radiation loss versus distance between the outer edge of the bend and the vertical external boundary.

VI. Conclusion

In this paper, a full vector analysis of optical dielectric waveguide bends using the finite-difference method has been developed. The formulation was based on the electric field components, E_r and E_z. For the complete set of the boundary conditions at each dielectric interface, the continuity of E_θ, H_θ, and the tangential component of the electric field, and the discontinuity of the normal component of the electric field were satisfied. The finite-difference scheme was modified to implement these boundary conditions.

To test the method, the field distributions of the bend whose layer structure is shown in Fig. 1 were calculated with various radii of curvature and the losses were also calculated. Our result shows that for the radius of curvature larger than 200 μm, the radiation loss of the 90° waveguide bend, whose layer structure is shown in Fig. 1, is smaller than 1 dB, and it shows the possibility that the waveguide bends can be substituted for the turning mirrors with comparable loss.

In our result, it is also shown that by applying optimal offsets at the conjunctions between the straight waveguide and the waveguide bend, the transition loss can be minimized. For example, if the optimal offset is applied, the transition loss of the bend with 150 μm radius can be reduced by approximately 4 dB.

Appendix

As shown in Fig. 8, the cross section of the curved waveguide was divided into small square cells to set up the finite-difference scheme. The field distributions are calculated at each grid point in the middle of the cell and in each cell, it is assumed that the refractive index is constant. The grid points are separated by constant step length both in r direction and z direction and each internal interface is placed halfway between adjacent grid points. The boundary conditions mentioned in Section III will be set at these internal interface. All situations are same with those in Stern's work [8].

At all internal interfaces, E_θ and H_θ should be continuous. E_θ and H_θ can be expressed in terms of Ψ and ϕ by

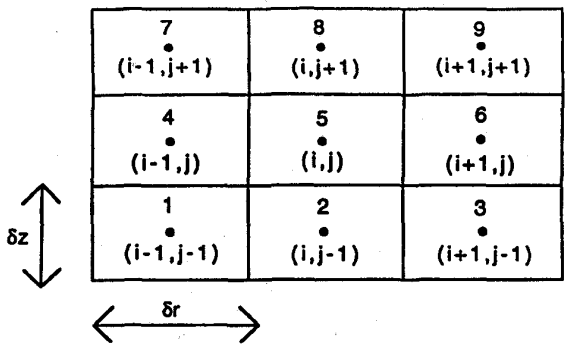

Fig. 8. Grid in the cross section of waveguide bend.

substituting $\Psi = rE_r$, $\phi = E_z$ into (9) and (11).

$$E_\theta = -\frac{j}{\nu}\left(\frac{\partial \psi}{\partial r} + r\frac{\partial \phi}{\partial z}\right) \tag{A1}$$

$$H_\theta = \frac{j}{\omega\mu_0}\left(\frac{1\partial \psi}{r\,\partial z} - \frac{\partial \phi}{\partial r}\right). \tag{A2}$$

Consider the interface between 5 and 6 cells, and from the discontinuity of E_r, we can construct the condition

$$n_{i,j}^2 \psi_{i+1/2,j}^{(5)} = n_{i+1,j}^2 \psi_{i+1/2,j}^{(6)} \tag{A3}$$

and from the continuity E_z, E_θ, and H_θ

$$\phi_{i+1/2,j}^{(5)} = \phi_{i+1/2,j}^{(6)} \tag{A4}$$

$$E_{\theta i+1/2,j}^{(5)} = E_{\theta i+1/2,j}^{(6)} \tag{A5}$$

$$H_{\theta i+1/2,j}^{(5)} = H_{\theta i+1/2,j}^{(6)}. \tag{A6}$$

By using the first-order approximation of Taylor series, we obtain

$$\psi_{i+1,j} = \psi_{i+1/2,j}^{(6)} + \frac{\delta r \partial \psi^{(6)}}{2\partial r_{i+1/2,j}} \tag{A7}$$

$$\psi_{i,j}^* = \psi_{i+1/2,j}^{(6)} - \frac{\delta r\, \partial \psi^{(6)}}{2\partial r_{i+1/2,j}} \tag{A8}$$

$$\psi_{i+1,j}^* = \psi_{i+1/2,j}^{(5)} + \frac{\delta r\, \partial \psi^{(5)}}{2\partial r_{i+1/2,j}} \tag{A9}$$

$$\psi_{i,j} = \psi_{i+1/2,j}^{(5)} - \frac{\delta r\, \partial \psi^{(5)}}{2\partial r_{i+1/2,j}} \tag{A10}$$

where $\psi_{i,j}^*$ and $\psi_{i+1,j}^*$ are spurious field values seen from cell 6 and from cell 5, respectively. From the above equations, we obtain

$$\psi_{i+1/2,j}^{(6)} = \frac{\psi_{i+1,j} + \psi_{i,j}^*}{2} \tag{A11}$$

$$\psi_{i+1/2,j}^{(5)} = \frac{\psi_{i+1,j}^* + \psi_{i,j}}{2} \tag{A12}$$

$$\frac{\partial \psi^{(6)}}{\partial r_{i+1/2,j}} = \frac{\psi_{i+1,j} - \psi_{i,j}^*}{\delta r} \tag{A13}$$

$$\frac{\partial \psi^{(5)}}{\partial r_{i+1/2,j}} = \frac{\psi_{i+1,j}^* - \psi_{i,j}}{\delta r}. \tag{A14}$$

By substituting (A11), (A12) into (A5), (A6), we obtain

$$\psi_{i,j}^* = \frac{n_{i,j}^2}{n_{i+1,j}^2}(\psi_{i+1,j}^* + \psi_{i,j}) - \psi_{i+1,j}. \tag{A15}$$

By substituting (A15) into (A13), we obtain

$$\frac{\partial \psi^{(6)}}{\partial r_{i+1/2,j}} = \left[2\psi_{i+1,j} - \frac{n_{i,j}^2}{n_{i+1,j}^2}(\psi_{i+1,j}^* + \psi_{i,j})\right]. \tag{A16}$$

By similar procedures for ϕ, we can obtain

$$\frac{\partial \phi^{(5)}}{\partial r_{i+1/2,j}} = \frac{\phi_{i+1,j}^* - \phi_{i,j}}{\delta r} \tag{A17}$$

$$\frac{\partial \phi^{(6)}}{\partial r_{i+1/2,j}} = \frac{2\phi_{i+1,j} - \phi_{i+1,j}^* - \phi_{i,j}}{\delta r}. \tag{A18}$$

The slight difference between (A16) and (A18) came from the continuity condition, (A4).

To set up the boundary conditions (A5) and (A6), we need to express the derivatives of Ψ and ϕ with respect to z. We can approximately write

$$\frac{\partial \psi^{(5)}}{\partial z_{i+1/2,j}} = \frac{\psi_{i+1/2,j+1}^{(5)} - \psi_{i+1/2,j-1}^{(5)}}{2\delta z} \tag{A19}$$

$$\frac{\partial \psi^{(6)}}{\partial z_{i+1/2,j}} = \frac{\psi_{i+1/2,j+1}^{(6)} - \psi_{i+1/2,j-1}^{(6)}}{2\delta z} \tag{A20}$$

and (A21) and (A22) shown at the top of the next page.

Above equations are obtained from the analogy with (A31)–(A34) by ignoring coupling terms. Now, by satisfying the boundary conditions (A5), (A6), we obtain

$$\begin{aligned}
\psi_{i+1,j}^* = {} & \frac{2n_{i+1,j}^2}{n_{i,j}^2 + n_{i+1,j}^2}\psi_{i+1,j} + \frac{n_{i+1,j}^2 - n_{i,j}^2}{n_{i,j}^2 + n_{i+1,j}^2}\psi_{i,j} \\
& + \frac{n_{i+1,j}^2}{n_{i,j}^2 + n_{i+1,j}^2}\frac{r\,\delta r}{4\delta z} \\
& \cdot \left[\left(\frac{2n_{i+1,j+1}^2}{n_{i+1,j}^2 + n_{i+1,j+1}^2} - \frac{2n_{i,j+1}^2}{n_{i,j}^2 + n_{i,j+1}^2}\right)\right. \\
& \cdot (\phi_{i,j+1} + \phi_{i+1,j+1}) \\
& + \left(\frac{n_{i+1,j+1}^2 - n_{i+1,j}^2}{n_{i+1,j}^2 + n_{i+1,j+1}^2} - \frac{n_{i,j+1}^2 - n_{i,j}^2}{n_{i,j}^2 + n_{i,j+1}^2}\right. \\
& \left. - \frac{n_{i+1,j-1}^2 - n_{i+1,j}^2}{n_{i+1,j}^2 + n_{i+1,j-1}^2} + \frac{n_{i,j-1}^2 - n_{i,j}^2}{n_{i,j}^2 + n_{i,j-1}^2}\right) \\
& \cdot (\phi_{i,j} + \phi_{i+1,j}) \\
& - \left(\frac{2n_{i+1,j-1}^2}{n_{i+1,j}^2 + n_{i+1,j-1}^2} - \frac{2n_{i,j-1}^2}{n_{i,j}^2 + n_{i,j-1}^2}\right) \\
& \left. \cdot (\phi_{i,j-1} + \phi_{i+1,j-1})\right]
\end{aligned} \tag{A23}$$

$$\phi_{i+1,j}^* = \phi_{i+1,j} + \frac{\delta r}{4r\,\delta z}\left\{\frac{2n_{i,j+1}^2 n_{i+1,j+1}^2}{n_{i,j+1}^2 + n_{i+1,j+1}^2}\right.$$

$$\frac{\partial \phi^{(5)}}{\partial z_{i+1/2,j}} = \frac{\dfrac{2n_{i,j+1}^2}{n_{i,j}^2+n_{i,j+1}^2}\phi_{i+1/2,j+1}^{(5)} - \dfrac{2n_{i,j-1}^2}{n_{i,j}^2+n_{i,j-1}^2}\phi_{i+1/2,j-1}^{(5)} + \left(\dfrac{n_{i,j+1}^2-n_{i,j}^2}{n_{i,j}^2+n_{i,j+1}^2} - \dfrac{n_{i,j-1}^2-n_{i,j}^2}{n_{i,j}^2+n_{i,j-1}^2}\right)\phi_{i+1/2,j}^{(5)}}{2\delta z} \tag{A21}$$

$$\frac{\partial \phi^{(6)}}{\partial z_{i+1/2,j}} = \frac{\dfrac{2n_{i+1,j+1}^2}{n_{i+1,j}^2+n_{i+1,j+1}^2}\phi_{i+1/2,j+1}^{(6)} - \dfrac{2n_{i+1,j-1}^2}{n_{i+1,j}^2+n_{i+1,j-1}^2}\phi_{i+1/2,j-1}^{(6)} + \left(\dfrac{n_{i+1,j+1}^2-n_{i+1,j}^2}{n_{i+1,j}^2+n_{i+1,j+1}^2} - \dfrac{n_{i+1,j-1}^2-n_{i+1,j}^2}{n_{i+1,j}^2+n_{i+1,j-1}^2}\right)\phi_{i+1/2,j}^{(6)}}{2\delta z}. \tag{A22}$$

$$\cdot\left(\frac{1}{n_{i,j}^2+n_{i,j+1}^2} - \frac{1}{n_{i+1,j}^2+n_{i+1,j+1}^2}\right)\cdot(\psi_{i,j+1}+\psi_{i+1,j+1}) + \frac{1}{n_{i,j}^2+n_{i+1,j}^2}\cdot\left[n_{i+1,j}^2\left(\frac{n_{i,j+1}^2-n_{i,j}^2}{n_{i,j}^2+n_{i,j+1}^2} - \frac{n_{i,j-1}^2-n_{i,j}^2}{n_{i,j-1}^2+n_{i,j}^2}\right) - n_{i,j}^2\left(\frac{n_{i+1,j+1}^2-n_{i+1,j}^2}{n_{i+1,j}^2+n_{i+1,j+1}^2} - \frac{n_{i+1,j-1}^2-n_{i+1,j}^2}{n_{i+1,j-1}^2+n_{i+1,j}^2}\right)\right]\cdot(\psi_{i,j}+\psi_{i+1,j}) - \frac{2n_{i,j-1}^2 n_{i+1,j-1}^2}{n_{i,j-1}^2+n_{i+1,j-1}^2}\cdot\left(\frac{1}{n_{i,j-1}^2+n_{i,j}^2} - \frac{1}{n_{i+1,j-1}^2+n_{i+1,j}^2}\right)\cdot(\psi_{i,j-1}+\psi_{i-1,j-1})\Bigg\}. \tag{A24}$$

If the same boundary conditions were set at the interface between cell 4 and cell 5, we obtain

$$\psi_{i-1,j}^* = \frac{2n_{i-1,j}^2}{n_{i-1,j}^2+n_{i,j}^2}\psi_{i-1,j} + \frac{n_{i-1,j}^2-n_{i,j}^2}{n_{i-1,j}^2+n_{i,j}^2}\psi_{i,j} + \frac{n_{i-1,j}^2}{n_{i-1,j}^2+n_{i,j}^2}\frac{r\,\delta r}{4\delta z}\cdot\left[\left(\frac{2n_{i,j+1}^2}{n_{i,j}^2+n_{i,j+1}^2} - \frac{2n_{i-1,j+1}^2}{n_{i-1,j}^2+n_{i-1,j+1}^2}\right)\cdot(\phi_{i-1,j+1}+\phi_{i,j+1}) + \left(\frac{n_{i,j+1}^2-n_{i,j}^2}{n_{i,j}^2+n_{i,j+1}^2} - \frac{n_{i-1,j+1}^2-n_{i-1,j}^2}{n_{i-1,j}^2+n_{i-1,j+1}^2} - \frac{n_{i,j-1}^2-n_{i,j}^2}{n_{i,j}^2+n_{i,j-1}^2} + \frac{n_{i-1,j-1}^2-n_{i-1,j}^2}{n_{i-1,j}^2+n_{i-1,j-1}^2}\right)\cdot(\phi_{i-1,j}+\phi_{i,j}) - \left(\frac{2n_{i,j-1}^2}{n_{i,j}^2+n_{i,j-1}^2} - \frac{2n_{i-1,j-1}^2}{n_{i-1,j}^2+n_{i-1,j-1}^2}\right)\cdot(\phi_{i-1,j-1}+\phi_{i,j-1})\right] \tag{A25}$$

$$\phi_{i-1,j}^* = \phi_{i-1,j} + \frac{\delta r}{4r\,\delta z}\Bigg\{\frac{2n_{i-1,j+1}^2 n_{i,j+1}^2}{n_{i-1,j+1}^2+n_{i,j+1}^2}\cdot\left(\frac{1}{n_{i-1,j}^2+n_{i-1,j+1}^2} - \frac{1}{n_{i,j}^2+n_{i,j+1}^2}\right)\cdot(\psi_{i-1,j+1}+\psi_{i,j+1}) + \frac{1}{n_{i-1,j}^2+n_{i,j}^2}\cdot\left[n_{i,j}^2\left(\frac{n_{i-1,j+1}^2-n_{i-1,j}^2}{n_{i-1,j}^2+n_{i-1,j+1}^2} - \frac{n_{i-1,j-1}^2-n_{i-1,j}^2}{n_{i-1,j-1}^2+n_{i-1,j}^2}\right) - n_{i-1,j}^2\left(\frac{n_{i,j+1}^2-n_{i,j}^2}{n_{i,j}^2+n_{i,j+1}^2} - \frac{n_{i,j-1}^2-n_{i,j}^2}{n_{i,j-1}^2+n_{i,j}^2}\right)\right]\cdot(\psi_{i-1,j}+\psi_{i,j}) - \frac{2n_{i-1,j-1}^2 n_{i,j-1}^2}{n_{i-1,j-1}^2+n_{i,j-1}^2}\cdot\left(\frac{1}{n_{i-1,j-1}^2+n_{i-1,j}^2} - \frac{1}{n_{i,j-1}^2+n_{i,j}^2}\right)\cdot(\psi_{i-1,j-1}+\psi_{i,j-1})\Bigg\} \tag{A26}$$

where $\psi_{i-1,j}^*$ and $\phi_{i-1,j}^*$ are spurious fields seen from cell 5.

So far, we have considered the boundary conditions set up at the vertical interfaces. Now, let's consider the horizontal interface between cell 8 and cell 5. From the discontinuity of E_z, we can construct the condition

$$n_{i,j}^2\phi_{i,j+1/2}^{(5)} = n_{i,j+1}^2\phi_{i,j+1/2}^{(8)} \tag{A27}$$

and from the continuity E_r, E_θ, and H_θ

$$\psi_{i,j+1/2}^{(5)} = \psi_{i,j+1/2}^{(8)} \tag{A28}$$

$$E_{\theta i,j+1/2}^{(5)} = E_{\theta i,j+1/2}^{(8)}. \tag{A29}$$

$$H^{(5)}_{\theta i,\,j+1/2} = H^{(8)}_{\theta i,\,j+1/2}. \tag{A30}$$

Then, by a similar analysis as before at the interface between cell 5 and 6, we obtain

$$\begin{aligned}
\psi^*_{i,\,j+1} = {} & \psi_{i,\,j+1} + \frac{r\,\delta z}{4\delta r}\left\{\frac{2n^2_{i+1,\,j}n^2_{i+1,\,j+1}}{n^2_{i+1,\,j}+n^2_{i+1,\,j+1}}\right. \\
& \cdot\left(\frac{1}{n^2_{i,\,j}+n^2_{i+1,\,j}} - \frac{1}{n^2_{i,\,j+1}+n^2_{i+1,\,j+1}}\right) \\
& \cdot(\phi_{i+1,\,j}+\phi_{i+1,\,j+1}) + \frac{1}{n^2_{i,\,j}+n^2_{i,\,j+1}} \\
& \cdot\left[n^2_{i,\,j+1}\left(\frac{n^2_{i+1,\,j}-n^2_{i,\,j}}{n^2_{i,\,j}+n^2_{i+1,\,j}} - \frac{n^2_{i-1,\,j}-n^2_{i,\,j}}{n^2_{i-1,\,j}+n^2_{i,\,j}}\right)\right. \\
& \left.- n^2_{i,\,j}\left(\frac{n^2_{i+1,\,j+1}-n^2_{i,\,j+1}}{n^2_{i,\,j+1}+n^2_{i+1,\,j+1}} - \frac{n^2_{i-1,\,j+1}-n^2_{i,\,j+1}}{n^2_{i-1,\,j+1}+n^2_{i,\,j+1}}\right)\right] \\
& \cdot(\phi_{i,\,j}+\phi_{i,\,j+1}) - \frac{2n^2_{i-1,\,j}n^2_{i-1,\,j+1}}{n^2_{i-1,\,j}+n^2_{i-1,\,j+1}} \\
& \cdot\left(\frac{1}{n^2_{i-1,\,j}+n^2_{i,\,j}} - \frac{1}{n^2_{i-1,\,j+1}+n^2_{i,\,j+1}}\right) \\
& \left.\cdot(\phi_{i-1,\,j}+\phi_{i-1,\,j+1})\right\}
\end{aligned} \tag{A31}$$

$$\begin{aligned}
\phi^*_{i,\,j+1} = {} & \frac{2n^2_{i,\,j+1}}{n^2_{i,\,j}+n^2_{i,\,j+1}}\,\phi_{i,\,j+1} + \frac{n^2_{i,\,j+1}-n^2_{i,\,j}}{n^2_{i,\,j}+n^2_{i,\,j+1}}\,\phi_{i,\,j} \\
& + \frac{n^2_{i,\,j+1}}{n^2_{i,\,j}+n^2_{i,\,j+1}}\,\frac{\delta z}{4\delta r} \\
& \cdot\left[\left(\frac{2n^2_{i+1,\,j+1}}{n^2_{i,\,j+1}+n^2_{i+1,\,j+1}} - \frac{2n^2_{i+1,\,j}}{n^2_{i,\,j}+n^2_{i+1,\,j}}\right)\right. \\
& \cdot(\psi_{i+1,\,j}+\psi_{i+1,\,j+1}) \\
& + \left(\frac{n^2_{i+1,\,j+1}-n^2_{i,\,j+1}}{n^2_{i+1,\,j+1}+n^2_{i,\,j+1}} - \frac{n^2_{i+1,\,j}-n^2_{i,\,j}}{n^2_{i+1,\,j}+n^2_{i,\,j}}\right. \\
& \left.- \frac{n^2_{i-1,\,j+1}-n^2_{i,\,j+1}}{n^2_{i-1,\,j+1}+n^2_{i,\,j+1}} + \frac{n^2_{i-1,\,j}-n^2_{i,\,j}}{n^2_{i-1,\,j}+n^2_{i,\,j}}\right) \\
& \cdot(\psi_{i,\,j}+\psi_{i,\,j+1}) \\
& - \left(\frac{2n^2_{i-1,\,j+1}}{n^2_{i-1,\,j+1}+n^2_{i,\,j+1}} - \frac{2n^2_{i-1,\,j}}{n^2_{i,\,j}+n^2_{i-1,\,j}}\right) \\
& \left.\cdot(\psi_{i-1,\,j}+\psi_{i-1,\,j+1})\right].
\end{aligned} \tag{A32}$$

From the same kind of boundary condition set at the interface between cell 2 and 5, we obtain

$$\begin{aligned}
\psi^*_{i,\,j-1} = {} & \psi_{i,\,j-1} + \frac{r\delta z}{4\delta r}\left\{\frac{2n^2_{i+1,\,j-1}n^2_{i+1,\,j}}{n^2_{i+1,\,j-1}+n^2_{i+1,\,j}}\right. \\
& \cdot\left(\frac{1}{n^2_{i,\,j-1}+n^2_{i+1,\,j-1}} - \frac{1}{n^2_{i,\,j}+n^2_{i,\,j+1}}\right) \\
& \cdot(\phi_{i+1,\,j-1}+\phi_{i+1,\,j}) + \frac{1}{n^2_{i,\,j-1}+n^2_{i,\,j}} \\
& \cdot\left[n^2_{i,\,j}\left(\frac{n^2_{i+1,\,j-1}-n^2_{i,\,j-1}}{n^2_{i+1,\,j-1}+n^2_{i,\,j-1}} - \frac{n^2_{i-1,\,j-1}-n^2_{i,\,j-1}}{n^2_{i-1,\,j-1}+n^2_{i,\,j-1}}\right)\right. \\
& \left.- n^2_{i,\,j-1}\left(\frac{n^2_{i+1,\,j}-n^2_{i,\,j}}{n^2_{i+1,\,j}+n^2_{i,\,j}} - \frac{n^2_{i-1,\,j}-n^2_{i,\,j}}{n^2_{i-1,\,j}+n^2_{i,\,j}}\right)\right] \\
& \cdot(\phi_{i,\,j-1}+\phi_{i,\,j}) - \frac{2n^2_{i-1,\,j-1}n^2_{i-1,\,j}}{n^2_{i-1,\,j-1}+n^2_{i-1,\,j}} \\
& \cdot\left(\frac{1}{n^2_{i-1,\,j-1}+n^2_{i,\,j-1}} - \frac{1}{n^2_{i-1,\,j}+n^2_{i,\,j}}\right) \\
& \left.\cdot(\phi_{i-1,\,j-1}+\phi_{i-1,\,j})\right\}
\end{aligned} \tag{A33}$$

$$\begin{aligned}
\phi^*_{i,\,j-1} = {} & \frac{2n^2_{i,\,j-1}}{n^2_{i,\,j-1}+n^2_{i,\,j}}\,\phi_{i,\,j-1} + \frac{n^2_{i,\,j-1}-n^2_{i,\,j}}{n^2_{i,\,j-1}+n^2_{i,\,j}}\,\phi_{i,\,j} \\
& + \frac{n^2_{i,\,j-1}}{n^2_{i,\,j-1}+n^2_{i,\,j}}\,\frac{\delta z}{4\delta r} \\
& \cdot\left[\left(\frac{2n^2_{i+1,\,j}}{n^2_{i,\,j}+n^2_{i+1,\,j}} - \frac{2n^2_{i+1,\,j-1}}{n^2_{i,\,j-1}+n^2_{i+1,\,j-1}}\right)\right. \\
& \cdot(\psi_{i+1,\,j-1}+\psi_{i+1,\,j}) \\
& + \left(\frac{n^2_{i+1,\,j}-n^2_{i,\,j}}{n^2_{i+1,\,j}+n^2_{i,\,j}} - \frac{n^2_{i+1,\,j-1}-n^2_{i,\,j-1}}{n^2_{i+1,\,j-1}+n^2_{i,\,j-1}}\right. \\
& \left.- \frac{n^2_{i-1,\,j}-n^2_{i,\,j}}{n^2_{i-1,\,j}+n^2_{i,\,j}} + \frac{n^2_{i-1,\,j-1}-n^2_{i,\,j-1}}{n^2_{i-1,\,j-1}+n^2_{i,\,j-1}}\right) \\
& \cdot(\psi_{i,\,j-1}+\psi_{i,\,j}) \\
& - \left(\frac{2n^2_{i-1,\,j}}{n^2_{i-1,\,j}+n^2_{i,\,j}} - \frac{2n^2_{i-1,\,j-1}}{n^2_{i,\,j-1}+n^2_{i-1,\,j-1}}\right) \\
& \left.\cdot(\psi_{i-1,\,j-1}+\psi_{i-1,\,j})\right].
\end{aligned} \tag{A34}$$

Now, modified finite-difference scheme can be obtained

$$\frac{\partial\psi}{\partial r_{i,\,j}} = \frac{\psi^*_{i+1,\,j}-\psi^*_{i-1,\,j}}{2\delta r} \tag{A35}$$

$$\frac{\partial^2\psi}{\partial r^2_{i,\,j}} = \frac{\psi^*_{i+1,\,j}-2\psi_{i,\,j}+\psi^*_{i-1,\,j}}{(\delta r)^2} \tag{A36}$$

$$\frac{\partial^2\psi}{\partial z^2_{i,\,j}} = \frac{\psi^*_{i,\,j+1}-2\psi_{i,\,j}+\psi^*_{i,\,j-1}}{(\delta z)^2}. \tag{A37}$$

Same modification can be obtained for ϕ by replacing Ψ with ϕ in above equations. Using this finite-difference scheme, we can discretize the differential equations (15) and (16) in Section II. It can be easily found that this approximate finite-difference scheme reduces to the normal scheme (which is not using spurious field) when all refractive indexes of the adjacent cells are same.

REFERENCES

[1] E. A. J. Marcatili, "Bends in optical dielectric guides," *Bell Syst. Technol. J.,* vol. 48, pp. 2103–2132, 1969.

[2] M. Heiblum and J. H. Harris, "Analysis of curved waveguides by conformal transformation," *IEEE J. Quantum Electron.,* vol. QE-11, pp. 75–83, 1975.

[3] J. Gu, P. Besse, and H. Melchior, "Novel method for analysis of curved optical rib-waveguides," *Electron. Lett.,* vol. 25, pp. 278–280, Feb. 1989.

[4] ——, "Method of lines for the analysis of the propagation characteristics of curved optical waveguides," *IEEE J. Quantum Electron.,* vol. 27, pp. 531–537, Mar, 1991.

[5] C. Neubauer, R. März, and M. Shienle, "A comparison between finite element calculations and experimental result of InGaAsP/InP waveguides," *J. Lightwave Technol.,* vol. 8, pp. 1932–1936, Dec. 1990.

[6] M. Goshiba, K. Hyata, and M. Suzuki, "Approximate finite-element analysis of anisotropic optical waveguides," *Electron. Lett.,* vol. 18, pp. 411–413, May 1982

[7] T. Yamamoto and M. Koshiba, "Numerical analysis of curvature loss in optical waveguides by finite-element method," *J. Lightwave. Technol.,* vol. 11, pp. 1579–1583, Oct. 1993.

[8] M. S. Stern, "Semivectorial polarized finite difference method for optical waveguides with arbitrary index profiles," *IEE Proc.,* vol. 135, no. 1, pp. 56–63, Feb. 1988.

[9] J. Wilkinson, *The Algebraic Eigenvalue Problem.* New York: Clarendon, 1965.

[10] W. Pascher and R. Pregla, "Analysis of curved optical waveguides by the vectorial method of lines," in *Proc. Int. Conf. Integrated Optics Optical Fiber Commun.,* Paris, France, 1991, pp. 237–240.

[11] ——, "Vectorial analysis of bends in optical strip waveguides by the method of lines," *Radio Sci.,* vol. 28, no. 6, pp. 1229–1233, 1993.

[12] H. J. M. Bastiaansen, J. M. van der Keur, and H. Blok, "Rigourous, full-vectorial source-type integral equation analysis of circularly curved channel waveguides," *IEEE Microwave Theory Tech.,* vol. 43, pp. 401–409, Feb. 1995.

Sangin Kim, photograph and biography not available at the time of publication.

Anand Gopinath, photograph and biography not available at the time of publication.